Thermochimica Acta, 183 (1991) 215–243
Elsevier Science Publishers B.V., Amsterdam

Thermodynamic properties of phase transitions in malonic acid and its deuterated analogue [α,β]

Mari Fukai, Takasuke Matsuo and Hiroshi Suga

Department of Chemistry and Microcalorimetry Research Center, Faculty of Science, Osaka University, Toyonaka, Osaka 560 (Japan)

(Received 14 September 1990)

Abstract

The heat capacities of malonic acid and its fully deuterated analogue were measured from 13 to 371 K. Two first-order phase transitions were found in each compound, and their thermodynamic quantities were determined as follows: malonic acid, 47.3 K (14.80 J mol^{-1} and 0.313 J K^{-1} mol^{-1}) and 352.2 K (1.837 kJ mol^{-1} and 5.217 J K^{-1} mol^{-1}); malonic acid-d_4, 60.0 K (23.86 J mol^{-1} and 0.411 J K^{-1} mol^{-1}) and 348.0 K (1.810 kJ mol^{-1} and 5.201 J K^{-1} mol^{-1}). The transition entropies suggest displacive mechanisms for both transitions. The entropy changes of the high temperature transitions are explained by vibrational frequency changes at the transitions. The low temperature transitions have a martensitic nature: the intermediate β phase supercools partially and coexists with the lowest temperature γ phase in a limited temperature range. Hysteresis was also found at the high temperature transitions. The deuteration effects on the transition temperatures are discussed with a thermodynamic model and compared with those of other hydrogen-bonded substances.

INTRODUCTION

Malonic acid, $CH_2(COOH)_2$ (abbreviated here to MA), undergoes two phase transitions at 360 and 48 K. The former transition temperature was determined by DSC [1] and the latter by heat capacity measurement [2]. There are thus three crystalline phases, designated α (above 360 K), β (360–48 K) and γ (below 48 K).

The crystal structure of the β phase was determined by X-ray diffraction [3]. It belongs to the triclinic space group $P\bar{1}$ (C_i) with two molecules per unit cell. The molecules are arranged in a zigzag chain along the *c* axis with centrosymmetrical hydrogen-bonded dimer rings where two hydrogen bonds

[α] Paper presented at the Second Japan–China Joint Symposium on Calorimetry and Thermal Analysis, 30 May–1 June 1990, Osaka, Japan.
[β] Contribution No. 31 from the Microcalorimetry Research Center.

0040-6031/91/$03.50

link cyclically the carboxyl groups of adjacent molecules. The two dimer rings in the unit cell, nearly orthogonal to each other, are cyrstallographically non-equivalent and have slightly different geometries. IR and Raman spectra at 100 K supported this structure by characterizing the two dimer rings with different vibrational frequencies [4]. A recent structure determination by neutron diffraction [5] also confirmed the previous X-ray results [3] except that the two dimer rings have more similar geometries and the hydrogen bonds have identical lengths (0.2672 and 0.2673 nm).

An electron nuclear double resonance (ENDOR) study revealed that there are four magnetically non-equivalent acid protons at 4.2 K [6]. This was the first indication that the crystal symmetry changes through a phase transition occurring at a low temperature. Pigenet et al. ascertained the $\gamma \rightarrow \beta$ transition by measuring IR and Raman spectra at various low temperatures [7]. The spectral changes due to the transition are as follows. First, many lattice and molecular vibrational modes split below the transition temperature; in particular, doublets of the carboxylic dimer bands in the β phase are replaced by quadruplets in the γ phase, which is in agreement with the previous results by ENDOR [6]. Second, the mutual exclusion rule is preserved in the γ phase, indicating that the centre of symmetry still exists in the γ phase. A doubling of the unit cell at the $\beta \rightarrow \gamma$ transition explains consistently these observations, as suggested by Pigenet et al. [7], and was confirmed by a neutron diffraction experiment on fully deuterated malonic acid, $CD_2(COOD)_2$ (abbreviated to MA-*d*) [8]. The γ phase belongs to the same space group as the β phase, namely the triclinic $P\bar{1}$ (C_i) and the unit cell doubles along the *a* axis across the $\beta \rightarrow \gamma$ transition.

The $\beta \rightarrow \alpha$ transition has also been investigated by IR and Raman spectra [1,9]. The most significant change due to the transition is that many doublets of carboxylic dimer bands in the β phase merge into single bands above the transition temperature. Comparison of the IR and Raman spectra of the α phase shows a considerable gerade–ungerade splitting for the carboxylic bands. These results indicated that the two centrosymmetric dimer rings which are non-equivalent in the β phase become equivalent in the α phase. Since line broadening caused by disordered atoms or molecules was not observed in the spectra of the α phase, Villepin et al. suggested that the $\beta \rightarrow \alpha$ transition is driven by an overall rotation of the molecular chain about its long axis parallel to the *c* axis and leads to a monoclinic structure $C2/c$ (C_{2h}^6) which does not involve any disorder [9]. Recent neutron diffraction data of MA-*d* taken at 373 K, however, gave the orthorhombic space group *Pbcn* (D_{2h}^{14}) [10]. It is not clear whether or not the α phase is disordered, because the structure has not been refined.

As described above, the phase transitions in malonic acid have been investigated by vibrational spectra and structure analyses. However the thermodynamic aspects of the transitions have not been studied.

For MA-*d*, the transition temperatures have been reported to be 366 and 57 K in the spectroscopic [9] and neutron diffraction [8] studies respectively. The phase transitions in MA-*d* are accompanied by the same changes in the vibrational spectra as for MA [7,9]. Deuteration modifies the relative stability of different phases of a substance, and its effect is particularly significant in hydrogen-bonded substances.

In the present work, we measured the heat capacities of MA and MA-*d* to determine the thermodynamic properties of the two phase transitions and to examine the deuteration effect on the phase transitions.

EXPERIMENTAL

Commercial malonic acid (purity, greater than 98%) was recrystallized from an aqueous solution to obtain the calorimetric sample of MA. The chemical analysis gave C, 34.61% (calc. 34.63%) and H, 3.87% (calc. 3.87%). MA-*d* was prepared by repeated recrystallization of the purified MA from D_2O. Both acidic and methylenic hydrogen atoms are deuterated by this method, because the methylenic hydrogen atoms in MA have relatively high acidity due to the strong electron-withdrawing effect of the two adjacent carboxyl groups. The deuteration level of the sample was estimated to be 99.7% from the proton content of the recovered D_2O solvent, determined by NMR measurement.

The heat capacities of MA and MA-*d* were measured with an automatic adiabatic calorimeter [11,12] between 13 and 371 K. The sample masses were 3.90271 g and 3.49659 g for MA and MA-*d* respectively.

RESULTS AND DISCUSSION

Experimental results

The experimental molar heat capacities of MA and MA-*d* are plotted in Fig. 1 as a function of temperature. Two peaks due to the phase transitions were found in each compound at the following temperatures: MA, 47.3 K ($\gamma \rightarrow \beta$) and 352.2 K ($\beta \rightarrow \alpha$); MA-*d*, 60.0 K ($\gamma \rightarrow \beta$) and 348.0 K ($\beta \rightarrow \alpha$). These transition temperatures do not agree with the literature values [1,8,9] except the $\gamma \rightarrow \beta$ transition of MA which has been reported to be at 48 K [2]. The $\gamma \rightarrow \beta$ transition temperature of MA-*d* is higher by 3 K, and the $\beta \rightarrow \alpha$ transition temperatures are lower by 8 K and 18 K for MA and MA-*d* respectively, than those reported previously. The three references [1,8,9] do not describe how the transition points were determined. The large differences might be attributed to a difference in the magnitude of the temperature step between the earlier and present experiments. In the present

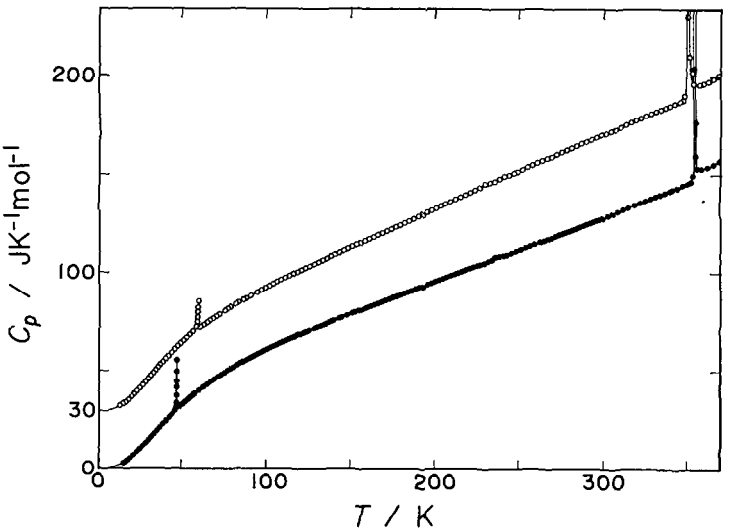

Fig. 1. Heat capacities of malonic acid and malonic acid-d_4: ●, malonic acid (MA); ○, malonic acid-d_4 (MA-d). The curve for MA-d is shifted upwards by 30 J K^{-1} mol^{-1} for clarity.

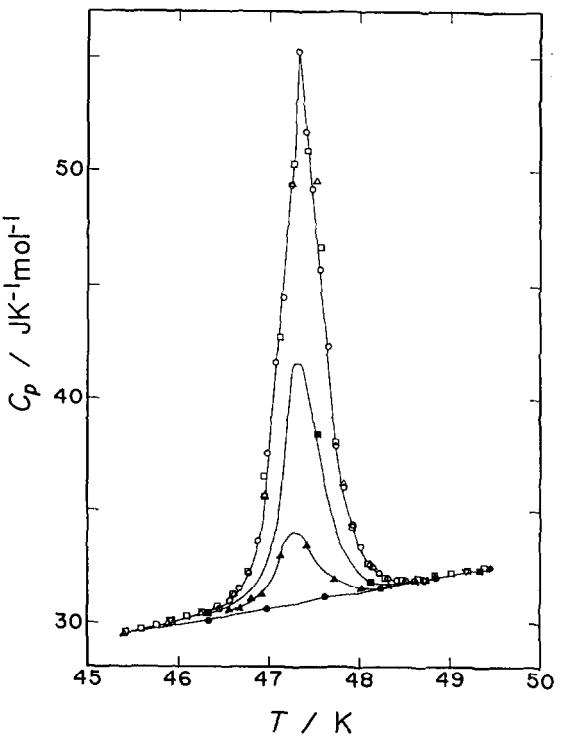

Fig. 2. Heat capacity of malonic acid (MA) near the $\gamma \rightarrow \beta$ transition under different precooling conditions: ▽, series 4; △, series 5; □, series 6; ▲, series 7; ○, series 8; ●, series 9; ■, series 10. The numerical values of the heat capacity and the chronological order of the measurements are given in Table 5 and Fig. 8 respectively.

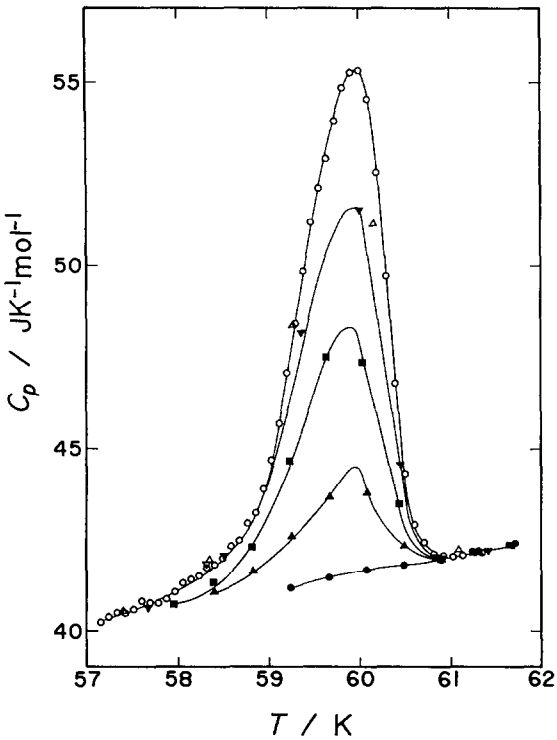

Fig. 3. Heat capacity of malonic acid-d_4 (MA-d) near the $\gamma \rightarrow \beta$ transition under different precooling conditions: △, series 4; ○, series 6; ▼, series 8; ▲, series 9; ▽, series 11; ●, series 14; ■, series 16. The numerical values of the heat capacity and the chronological order of the measurements are given in Table 6 and Fig. 9 respectively.

work, the temperature step in one heat capacity measurement was adjusted to be approximately 0.1 K and 1 K in the $\gamma \rightarrow \beta$ and $\beta \rightarrow \alpha$ transition regions respectively.

In both curves, there is another small anomaly around 230 K, the glass transition point of Teflon [13]. The small anomalies were caused by incomplete correction for the thermal anomaly of the polymer material used for electrical insulation in the sample cell, and they are not intrinsic to the samples.

As the measurement was repeated several times across the $\beta \rightarrow \alpha$ transition regions, the heat capacity values of the α phase deviated positively from the data in the previous measurement series. This phenomenon turned out to result from the partial decomposition of the sample and prevented the collection of equilibrium heat capacity data above 371 K.

Figures 2 and 3 display the heat capacities near the $\gamma \rightarrow \beta$ transitions for MA and MA-d respectively. The different series of data plotted as open marks agree very well. However, in the series denoted by solid marks, partial supercooling of the β phase was found. The anomalous heat capacities

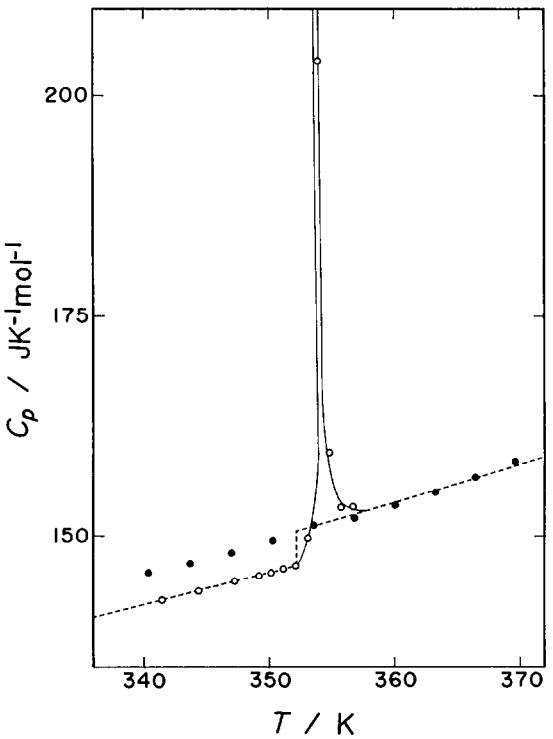

Fig. 4. Heat capacity of malonic acid (MA) near the $\beta \rightarrow \alpha$ transition: ○, series 16; ●, series 17.

depended on the precooling temperature, that is, the lowest temperature experienced by the sample before each series of measurement. This hysteresis will be discussed in the next section.

The heat capacity near the $\beta \rightarrow \alpha$ transition is shown in Fig. 4 for MA and in Fig. 5 for MA-*d*. At the $\beta \rightarrow \alpha$ transitions, the apparent heat capacities reached 1400 J K^{-1} mol^{-1} and 1900 J K^{-1} mol^{-1} in MA and MA-*d* respectively. Hysteresis was also found at this transition. Not only did the α phase supercool, as plotted by the solid circles in the figures, but the β phase also superheated. The dotted lines in the figures represent the normal heat capacity functions. The heat capacities of the α phases were larger than those of the β phases by 4.2 J K^{-1} mol^{-1} and 2.9 J K^{-1} mol^{-1} for MA and MA-*d* respectively, at "equilibrium" transition temperatures where the normal heat capacities have steps. The determination of the normal heat capacities and the "equilibrium" transition temperatures will be described later.

The observations on the supercooling of the α and β phases demonstrate that the $\beta \rightarrow \alpha$ and $\gamma \rightarrow \beta$ transitions are first order. In the $\beta \rightarrow \alpha$ transition regions, the time required for thermal equilibration increased to about an hour, compared with 1–5 min in the normal region. Slow equilibration is

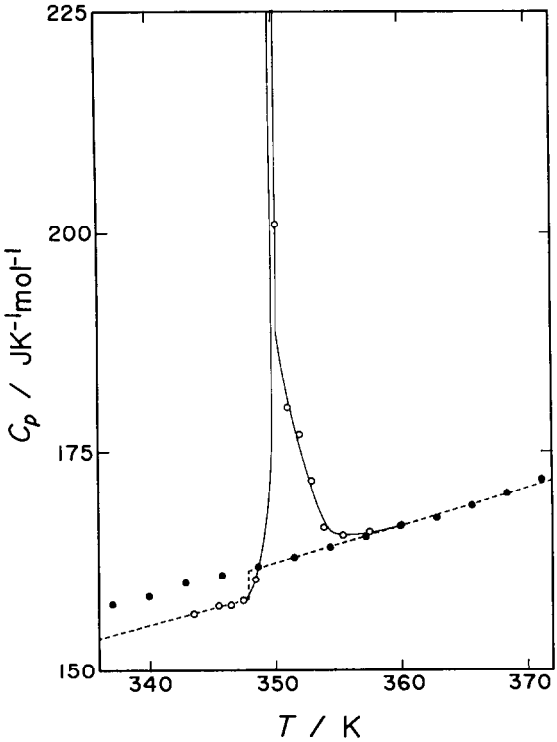

Fig. 5. Heat capacity of malonic acid-d_4 (MA-d) near the $\beta \rightarrow \alpha$ transition: ○, series 21; ●, series 22.

often observed in first-order transitions. In contrast, the thermal equilibration time did not change through the $\gamma \rightarrow \beta$ transitions, so that the heat capacity values could be obtained under thermal equilibrium conditions.

Selected heat capacity values of MA and MA-d are listed in order of increasing temperature in Tables 1 and 2 respectively.

Low temperature $\gamma \rightarrow \beta$ phase transitions

Determination of normal and excess heat capacities

In order to derive the enthalpies and entropies of the transitions, we decomposed the experimental heat capacities additively into the normal and transitional parts. The normal heat capacity consists of vibrational contributions and a small correction for thermal dilation. The vibrational part was assumed to be a sum of the Debye and Einstein heat capacities.

Malonic acid has 33 vibrational degrees of freedom. Most of the lattice and molecular vibrational frequencies have been determined from the IR and Raman spectra at 100 K [4]. We took 24 frequencies above 200 cm^{-1} from them for the normal heat capacity calculations, since a computation in which all the known frequencies were used did not converge satisfactorily.

TABLE 1

Selected heat capacity values of malonic acid

T (K)	C_p (J K^{-1} mol^{-1})	T (K)	C_p (J K^{-1} mol^{-1})	T (K)	C_p (J K^{-1} mol^{-1})	T (K)	C_p (J K^{-1} mol^{-1})
15.11	3.430	65.07	43.26	139.87	75.46	251.03	112.0
15.62	3.764	66.20	43.95	141.42	76.10	253.75	112.9
16.27	4.174	67.30	44.59	142.96	76.56	256.46	113.7
16.98	4.617	68.38	45.22	144.49	77.05	259.16	114.5
17.73	5.120	69.44	45.86	146.01	77.59	261.43	115.4
18.49	5.668	70.49	46.45	147.53	78.12	263.48	116.0
19.27	6.225	71.51	47.01	149.04	78.62	265.53	116.6
20.15	6.908	72.52	47.56	150.54	79.12	267.57	117.4
21.09	7.647	73.52	48.12	152.45	79.74	269.60	118.1
22.01	8.373	74.50	48.65	154.78	80.55	271.63	118.7
22.91	9.111	75.46	49.14	157.08	81.30	273.65	119.4
23.78	9.842	76.42	49.69	159.37	82.07	275.66	120.1
24.64	10.58	77.36	50.17	161.65	82.85	277.66	120.7
25.51	11.34	78.29	50.67	163.91	83.56	279.66	121.3
26.39	12.11	79.21	51.09	166.15	84.33	281.65	122.0
27.25	12.88	80.11	51.60	168.37	85.08	283.63	122.7
28.09	13.63	81.01	51.99	170.59	85.81	285.61	123.4
28.92	14.38	81.90	52.48	172.79	86.52	287.58	124.2
29.73	15.13	82.78	52.91	174.97	87.28	289.54	124.8
30.57	15.88	83.45	53.30	177.15	87.96	291.50	125.4
31.41	16.68	84.65	53.85	179.31	88.67	293.45	126.1
32.25	17.45	86.32	54.61	181.45	89.31	295.39	126.8
33.07	18.22	88.46	55.62	183.73	90.07	297.33	127.3
33.91	18.99	90.58	56.57	186.15	90.81	299.56	128.1
34.76	19.79	92.65	57.54	188.56	91.59	302.68	129.2
35.62	20.57	94.69	58.41	190.95	92.37	305.78	130.2
36.51	21.39	96.69	59.31	193.32	93.15	308.86	131.3
37.47	22.28	98.66	60.10	195.68	93.92	311.93	132.4
38.48	23.20	100.60	60.97	198.03	94.70	314.98	133.4
39.49	24.09	102.51	61.74	200.37	95.45	316.07	133.7
40.50	25.02	104.39	62.49	202.69	96.18	319.11	134.8
41.55	25.99	106.25	63.21	205.01	96.90	322.13	135.9
42.65	26.96	108.08	63.98	207.31	97.69	325.13	136.9
44.12	28.28	109.90	64.65	209.60	98.46	328.12	137.9
45.92	30.11	111.69	65.35	211.87	99.16	331.09	138.9
47.17	44.50	113.47	66.02	214.14	99.89	334.06	139.9
47.33	55.27	115.23	66.69	216.39	100.7	337.00	140.9
47.65	42.33	116.96	67.34	218.63	101.4	339.94	141.9
48.03	33.44	118.69	68.46	220.87	102.1	342.38	142.9
49.18	32.36	120.39	68.65	223.09	102.8	344.82	143.6
50.44	33.31	122.09	69.24	225.30	103.5	348.58	145.0
52.02	34.51	123.76	69.84	227.50	104.2	351.38	447.2
53.53	35.64	125.43	70.43	229.69	105.0	352.66	1447
54.98	36.69	127.08	71.02	231.87	106.1	354.70	176.5
56.38	37.67	128.72	71.64	234.04	106.6	358.21	153.1

TABLE 1 (continued)

T (K)	C_p (J K^{-1} mol^{-1})	T (K)	C_p (J K^{-1} mol^{-1})	T (K)	C_p (J K^{-1} mol^{-1})	T (K)	C_p (J K^{-1} mol^{-1})
57.73	38.59	130.35	72.21	236.20	108.0	361.84	153.9
59.04	39.46	131.96	72.72	238.35	108.4	365.45	155.3
60.31	40.29	133.56	73.28	241.01	108.8	369.04	157.1
61.54	41.08	135.16	73.87	242.78	109.2		
62.75	41.81	136.74	74.45	245.54	110.1		
63.92	42.60	138.31	74.92	248.30	111.1		

The nine remaining unknown frequencies were determined by minimizing the following function:

$$F(\theta_{D,j}, \theta_{E,j}, A) = \Sigma_i \Big[C_p(T_i) - AT_i \{ C_p(T_i) \}^2 - C_{v,\text{known}}(T_i) - C_{v,\text{unknown}}(T_i) \Big]^2 \quad (1)$$

Here $C_p(T_i)$ is the experimental heat capacity and $AT_i\{C_p(T_i)\}^2$ is the $C_p - C_v$ correction term at $T = T_i$. $C_{v,\text{ known}}(T_i)$ is the Einstein heat capacity summed over the known vibrational modes and $C_{v,\text{unknown}}(T_i)$ is defined as follows:

$$C_{v,\text{unknown}}(T_i) = \Sigma_j \left[n_{D,j} RD(\theta_{D,j}/T_i) + n_{E,j} RE(\theta_{E,j}/T_i) \right] \quad (2)$$

where R is the gas constant, $D(\theta_{D,j}/T_i)$ is the Debye heat capacity of the characteristic temperature $\theta_{D,j}$ at $T = T_i$, $E(\theta_{E,j}/T_i)$ is the Einstein heat capacity of the characteristic temperature $\theta_{E,j}$ at $T = T_i$, and $n_{D,j}$ and $n_{E,j}$ are the weights of the Debye and Einstein modes respectively.

We used the experimental data which were regarded as free from the influence of the transition. The optimized parameters comprising the characteristic temperatures ($\theta_{D,j}$ and $\theta_{E,j}$) and the $C_p - C_v$ correction coefficient (A) were found by a non-linear least-squares method on a microcomputer. Results of the fitting are summarized in Table 3. Subtraction of the normal parts from the experimental heat capacities gave the excess heat capacities, as shown in Figs. 6 and 7. As can be seen from these figures, the transition region in MA-*d* is wider than that in MA. The excess heat capacity of MA increases abruptly at the transition point and has a very sharp peak. In MA-*d*, however, the transition starts already at 0.75 T_{trs} and progresses gradually thereafter. Such a precursory phenomenon of a phase transition is usually attributed to an impurity effect. However, this explanation is unlikely to apply in the present case, because the excess enthalpy gained in the pre-transition region is as large as 33% of the overall transition enthalpy. This effect seems to be too large to have been caused by the isotopic impurity (namely 0.3% of proton) or by other impurities, unless one assumes

TABLE 2

Selected heat capacity values of malonic acid-d_4

T (K)	C_p (J K^{-1} mol^{-1})	T (K)	C_p (J K^{-1} mol^{-1})	T (K)	C_p (J K^{-1} mol^{-1})	T (K)	C_p (J K^{-1} mol^{-1})
12.69	2.290	45.97	30.76	116.28	69.37	241.53	119.2
13.43	2.673	46.89	31.57	118.68	70.33	244.40	119.7
13.99	2.980	47.80	32.36	121.06	71.33	247.26	120.8
14.57	3.324	48.69	33.12	123.50	72.28	250.10	121.9
15.16	3.671	49.59	33.89	125.99	73.28	252.92	122.9
15.75	4.033	50.52	34.67	128.46	74.31	255.73	124.0
16.35	4.421	51.44	35.44	130.92	75.29	258.53	125.0
16.94	4.819	52.59	36.37	133.35	76.29	261.31	126.1
17.53	5.222	53.57	37.22	135.77	77.24	263.90	127.1
18.11	5.656	54.53	37.99	138.25	78.21	266.77	128.1
18.69	6.088	55.48	38.80	140.78	79.24	269.63	129.2
19.25	6.508	56.43	39.61	143.29	80.23	272.26	130.2
19.82	6.985	57.40	40.54	145.80	81.20	275.34	131.5
20.37	7.435	58.35	41.96	148.28	82.24	278.25	132.5
20.92	7.873	59.26	48.35	150.76	83.25	281.15	133.5
21.46	8.297	60.00	55.32	153.29	84.18	284.04	134.7
22.00	8.748	60.29	49.73	155.88	85.19	286.91	135.8
22.53	9.203	60.50	44.32	158.45	86.18	289.76	136.8
23.07	9.664	60.71	42.45	161.01	87.22	292.60	137.8
23.61	10.14	61.14	42.09	163.56	88.20	295.42	139.0
24.17	10.63	62.05	42.67	166.10	89.24	289.24	140.0
24.71	11.11	63.01	43.26	168.69	90.23	301.05	141.0
25.27	11.62	63.98	43.88	171.34	91.23	304.02	142.0
25.85	12.14	64.96	44.44	173.97	92.30	306.84	143.0
26.56	12.78	66.59	45.41	176.60	93.36	309.85	144.3
27.38	13.52	68.48	46.52	179.22	94.34	312.90	145.4
28.17	14.26	70.31	47.58	181.82	95.34	315.94	146.6
28.99	15.02	72.09	48.58	184.47	96.40	318.96	147.7
29.85	15.83	73.82	49.54	187.29	97.49	321.98	148.8
30.67	16.60	75.51	50.47	190.20	98.62	324.98	149.9
31.47	17.37	77.16	51.35	193.05	99.81	328.00	151.0
32.25	18.11	78.77	52.25	195.85	100.9	331.03	152.1
33.01	18.83	80.35	53.03	198.62	102.0	334.06	153.1
33.76	19.54	81.84	53.89	201.38	103.0	336.83	154.1
34.48	20.24	83.94	54.91	204.12	104.1	339.43	154.9
35.18	20.93	86.68	56.21	206.84	105.2	342.23	156.0
35.87	21.57	89.34	57.50	209.68	106.3	345.20	157.3
37.20	22.82	91.94	58.75	212.66	107.4	348.15	160.7
37.98	23.53	94.47	59.86	215.61	108.6	350.81	239.5
38.86	24.35	96.96	61.04	218.55	109.7	352.25	1878
39.77	25.19	99.41	62.15	221.46	110.9	353.43	361.9
40.66	26.01	101.82	63.15	224.36	112.1	355.76	174.4
41.54	26.81	104.20	64.26	227.24	113.3	358.59	166.3
42.42	27.60	106.55	65.26	230.10	115.3	361.46	167.2
43.31	28.40	108.96	66.27	232.95	116.0	364.31	168.4
44.18	29.16	111.43	67.32	235.78	116.5	367.12	169.7
45.06	29.95	113.87	68.32	238.64	117.9	369.89	170.9

TABLE 3

Optimized parameters of the normal heat capacity functions

$CH_2(COOH)_2$		$CD_2(COOD)_2$	
Temp. range (K)	No. of points used for fitting	Temp. range (K)	No. of points used for fitting
15.62–44.12	13	12.69–49.69	15
46.34–49.44 [a]	3 [a]	61.71–301.35	37
52.02–300.85	45		

$CH_2(COOH)_2$			$CD_2(COOD)_2$		
Parameter		Degeneracy	Parameter		Degeneracy
$\theta_{D,1}$ (K)	102.7 ± 0.8	2	$\theta_{D,1}$ (K)	119.7±0.4	3
$\theta_{D,2}$ (K)	425.2 ±26.8	1			
$\theta_{E,1}$ (K)	151.5 ± 2.2	3	$\theta_{E,1}$ (K)	174.8±0.8	4
$\theta_{E,2}$ (K)	192.0 ± 5.7	2	$\theta_{E,2}$ (K)	268.2±5.0	1
$\theta_{E,3}$ (K)	417.1 ±15.9	1	$\theta_{E,3}$ (K)	451.6±4.8	1
$A\times10^6$ (J^{-1} mol)	1.93± 0.01		$A\times10^6$ (J^{-1} mol)	1.07±0.01	

[a] Data in series 9 where the β phase was completely supercooled (see Fig. 2 and the text).

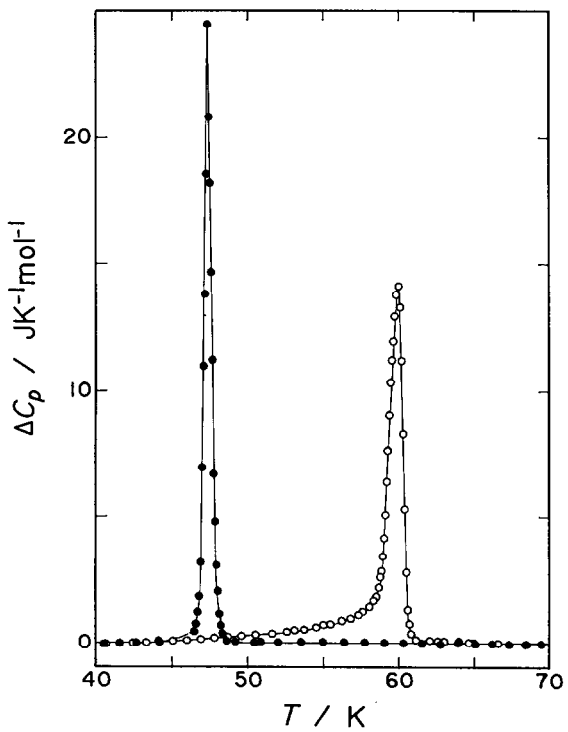

Fig. 6. Excess heat capacities of malonic acid and malonic acid-d_4 near the $\gamma \rightarrow \beta$ transitions: ●, malonic acid (MA); ○, malonic acid-d_4 (MA-d).

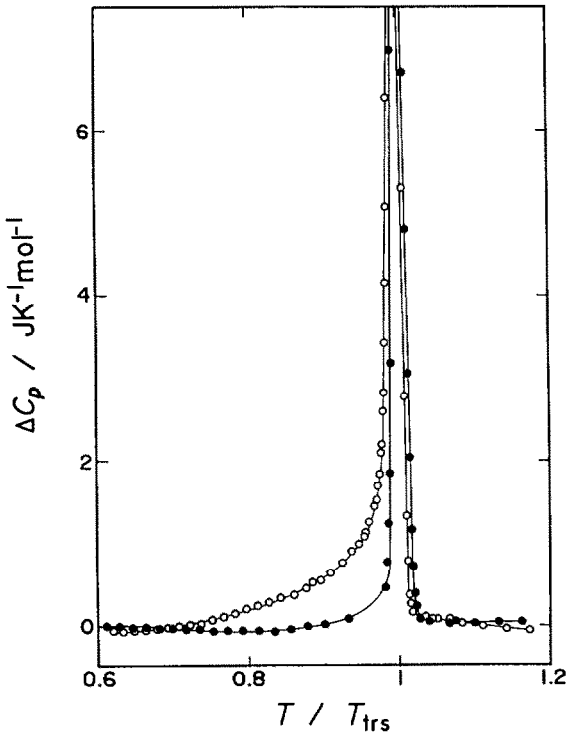

Fig. 7. Excess heat capacities of malonic acid and malonic acid-d_4 near the $\gamma \rightarrow \beta$ transitions plotted against the reduced temperature: ●, malonic acid (MA); ○, malonic acid-d_4 (MA-d).

an unrealistically effectual mechanism of the transition broadening by impurities. Hence this precursory phenomenon is probably an intrinsic deuteration effect.

Thermodynamic quantities of the $\gamma \rightarrow \beta$ transitions

We integrated the excess heat capacity taking account of the latent heat to obtain the transition enthalpy. The transition entropy was calculated similarly. The thermodynamic quantities of the $\gamma \rightarrow \beta$ transitions thus determined are listed in Table 4. The deuteration of MA raises not only the transition temperature but also the transition entropy. Relative increases in the transition temperature and entropy are 27% and 31% respectively. In the

TABLE 4

Thermodynamic quantities of the $\gamma \rightarrow \beta$ transitions in $CH_2(COOH)_2$ and $CD_2(COOD)_2$

	$CH_2(COOH)_2$	$CD_2(COOD)_2$
T_{trs} (K)	47.3	60.0
$\Delta_{trs}H$ (J mol^{-1})	14.80 ±0.17	23.86 ±0.14
$\Delta_{trs}S$ (J K^{-1} mol^{-1})	0.313±0.003	0.411±0.003

TABLE 5

Heat capacity of malonic acid near the $\gamma \rightarrow \beta$ transition under different precooling conditions [a]

T (K)	C_p (J K^{-1} mol^{-1})	T (K)	C_p (J K^{-1} mol^{-1})	T (K)	C_p (J K^{-1} mol^{-1})	T (K)	C_p (J K^{-1} mol^{-1})
Series 4		46.60	31.27	47.73	31.96	48.22	32.27
45.92	30.11	46.77	32.32	48.03	31.57	48.32	32.02
49.18	32.36	46.95	36.54	48.33	31.68	48.42	31.95
		47.12	42.72	48.62	31.90	48.52	31.93
Series 5		47.27	50.30			48.61	31.95
45.41	29.49	47.42	50.88	Series 8		48.71	32.01
45.89	29.97	47.57	46.68	46.46	30.60		
46.26	30.40	47.74	38.05	46.57	30.99	Series 9	
46.62	31.26	47.91	34.28	46.67	31.54	46.34	30.08
46.96	35.70	48.10	32.69	46.78	32.24	46.99	30.61
47.26	49.43	48.28	32.04	46.88	33.67	47.62	31.17
47.54	49.55	48.47	31.97	46.98	37.53	48.24	31.56
47.83	36.22	48.65	32.05	47.08	41.63	48.85	32.05
48.16	32.54	48.83	32.16	47.17	44.50	49.44	32.53
48.50	31.89	49.02	32.27	47.25	49.37		
48.83	32.08	49.20	32.39	47.33	55.27	Series 10	
		49.38	32.57	47.41	51.73	46.33	30.43
Series 6				47.49	49.21	46.96	35.66
45.42	29.61	Series 7		47.57	45.71	47.54	38.41
45.60	29.71	46.57	30.55	47.65	42.33	48.13	31.87
45.76	29.87	46.69	30.64	47.74	37.87	48.73	31.96
45.93	30.08	46.81	31.07	47.84	36.05	49.33	32.42
46.10	30.29	46.93	31.26	47.93	34.39		
46.26	30.46	47.13	33.01	48.03	33.44		
46.43	30.73	47.43	33.49	48.12	32.63		

[a] All the data in Table 5 are plotted in Fig. 2.

second-to-last section below, we will compare these magnitudes of the deuteration effect with those of other hydrogen-bonded substances to discuss the nature of the transitions. Both transition entropies are very small in comparison with R ln 2 (equal to 5.763 J K^{-1} mol^{-1}) which is the usual indicator of an order–disorder transition. This indicates that the $\gamma \rightarrow \beta$ transitions are of displacive type.

Hysteresis of the $\gamma \rightarrow \beta$ transitions

The $\gamma \rightarrow \beta$ transitions exhibited hysteresis as shown previously in Figs. 2 and 3. The numerical values of the heat capacities plotted in Figs. 2 and 3 are given in Tables 5 and 6 respectively, and the chronological order of the measurements is summarized in Figs. 8 and 9. In Fig. 3 for MA-*d*, the results of some measurement series have been omitted for the sake of clarity.

TABLE 6

Heat capacity of malonic acid-d_4 near the $\gamma \rightarrow \beta$ transition under different precooling conditions [a]

T (K)	C_p (J K^{-1} mol^{-1})	T (K)	C_p (J K^{-1} mol^{-1})	T (K)	C_p (J K^{-1} mol^{-1})	T (K)	C_p (J K^{-1} mol^{-1})
Series 4		58.67	42.50	61.03	42.05	Series 11	
57.40	40.54	58.76	42.97	61.14	42.09	58.32	41.84
58.35	41.96	58.85	43.26	61.24	42.20	61.70	42.39
59.26	48.35	58.94	43.91	61.35	42.16		
60.16	51.15	59.03	44.70			Series 14	
61.09	42.24	59.11	45.69	Series 8		59.24	41.18
		59.20	47.06	57.67	40.64	59.66	41.47
Series 6		59.29	48.40	58.51	42.09	60.08	41.68
57.15	40.23	59.38	49.85	59.36	48.14	60.49	41.82
57.24	40.38	59.47	51.20	60.00	51.55	60.90	41.97
57.33	40.49	59.55	52.12	60.45	44.57	61.31	42.22
57.42	40.48	59.64	52.92	60.92	42.03	61.71	42.43
57.51	40.58	59.73	53.95	61.42	42.23		
57.60	40.81	59.82	54.85			Series 16	
57.69	40.77	59.91	55.26	Series 9		57.95	40.73
57.78	40.75	60.00	55.32	58.40	41.06	58.39	41.33
57.87	40.87	60.10	54.54	58.83	41.65	58.81	42.32
57.96	41.07	60.19	52.54	59.25	42.62	59.23	44.68
58.05	41.31	60.29	49.73	59.67	43.69	59.63	47.49
58.14	41.42	60.39	46.78	60.08	43.80	60.03	47.35
58.23	41.51	60.50	44.32	60.49	42.35	60.43	43.50
58.32	41.74	60.60	42.93	60.91	41.98	60.84	42.03
58.41	41.82	60.71	42.45	61.32	42.18	61.24	42.17
58.49	42.01	60.82	42.12			61.65	42.38
58.59	42.33	60.92	42.08				

[a] All the data in Table 6 are plotted in Fig. 3.

It was found that the lower the precooling temperature, the larger the transitional heat capacity. This indicates that below the transition temperature, the stable γ phase and the supercooled metastable β phase coexisted to an extent which depended on the precooling temperature. The fraction of the γ phase, x_γ, was determined on the assumption that x_γ is proportional to the transition enthalpy in each series, and is plotted against the precooling temperature T^* in Figs. 10 and 11 for MA and MA-d respectively. The numbers attached to the data points identify the measurement series. Most of the series were measured immediately after the sample was cooled from above the transition temperature. However, for series 16 of MA-d, we started the measurement after annealing the sample at 57.73 K for 17.5 h. The result joined smoothly with the other points as shown in Fig. 11. This

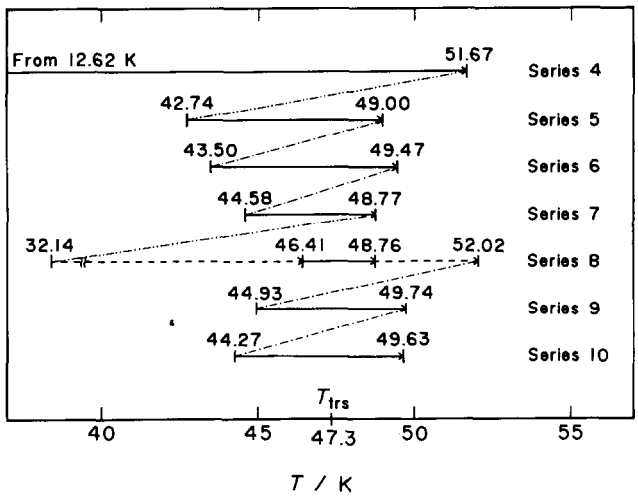

Fig. 8. Chronological order of the heat capacity measurement in the $\gamma \rightarrow \beta$ transition region of malonic acid (MA): ———, heat capacity measurement; — — —, heating; ·–·–·, rapid cooling; ··–···–··, gradual cooling. The results are plotted in Fig. 2.

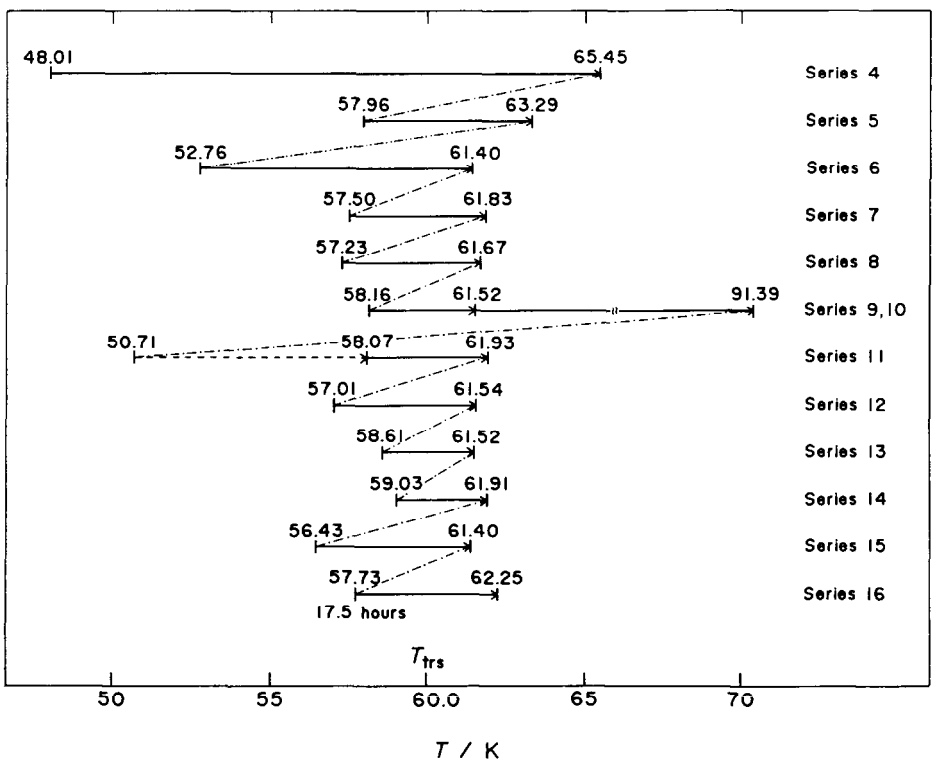

Fig. 9. Chronological order of the heat capacity measurement in the $\gamma \rightarrow \beta$ transition region of malonic acid-d_4 (MA-d): ———, heat capacity measurement; — — —, heating; ·–·–·, rapid cooling; ··–···–···, gradual cooling. Some of the results are plotted in Fig. 3.

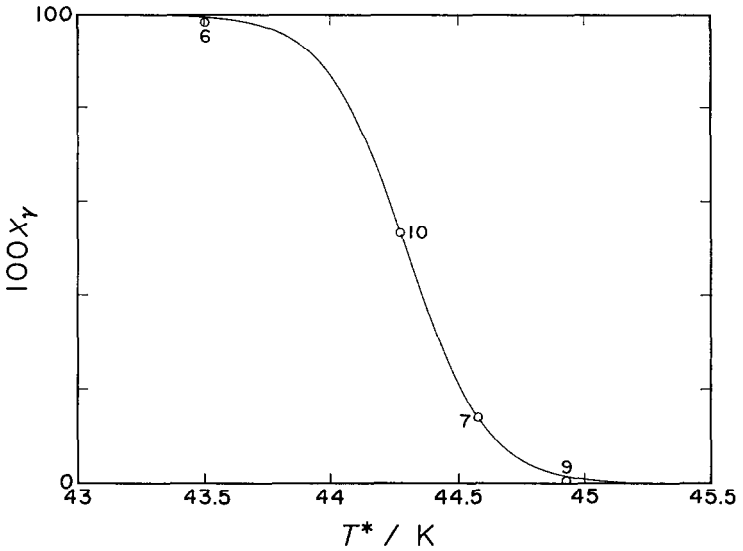

Fig. 10. Fraction of the γ phase vs. the precooling temperature for malonic acid (MA). The numbers attached to the data points identify the measurement series. The curve is the fitted function in eqn. (3) with the parameters given in Table 7.

proves that the proportion of the two coexisting phases is dependent only on the precooling temperature and independent of cooling rate or annealing.

One can see from Figs. 10 and 11 that the temperature range of the two-phase coexistence of MA-*d* (55–60 K) is twice as wide as that of MA

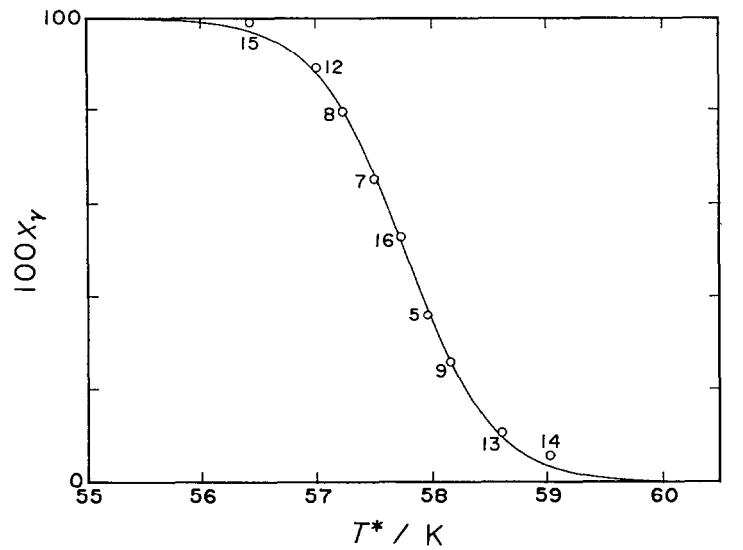

Fig. 11. Fraction of the γ phase vs. the precooling temperature for malonic acid-d_4 (MA-*d*). The numbers attached to the data points identify the measurement series. The curve is the fitted function in eqn. (3) with the parameters given in Table 7.

(43–45.5 K). In addition, the β phase of MA-*d* begins to transform into the γ phase just below the transition temperature (60.0 K), whereas the β phase of MA can supercool completely to 2 K below the transition point (47.3 K). The more gradual progress of the transition in MA-*d* may make it less susceptible to supercooling.

The coexistence of two phases over a temperature range is obviously contradictory to Gibbs' phase rule, and it cannot be understood within the framework of the thermodynamics of bulk phases. Similar phase transitions in which two phases coexist have been reported in $K_4[Fe(CN)_6] \cdot 3H_2O$, $K_4[Fe(CN)_6] \cdot 3D_2O$ [14], $(NH_4)_3[AlF_6]$ [15], NH_4Br [16], ND_4Br [17], $Fe[S_2CN(C_2H_5)_2]_2Br$ [18] and $(CH_3NH_3)_2[TeCl_6]$ [19].

In martensitic transitions, the driving force of the transition is the free energy difference between the high and low temperature phases, and the transition does not occur until the driving force reaches a threshold value. However, creation of the low temperature phase increases the threshold value and prevents further progress of the transition, so that the transition stops at an intermediate stage. It is interesting that the present phase transitions have two distinguishing properties of a martensitic transition. Firstly, the transition can be stopped at any intermediate stage by controlling the temperature to which the sample is cooled. Secondly, the apparent equilibrium is established rapidly in an intermediate stage and annealing thereafter at that temperature has practically no effect.

The precooling-temperature dependence of the fraction x_γ could be reproduced by the next function

$$x_\gamma = \left[1\text{-}\tanh\left(\frac{T^*\text{-}P(1)}{P(2)}\right)\right]/2 \tag{3}$$

The two fitting parameters $P(1)$ and $P(2)$, as given in Table 7, were calculated by the least-squares method, and the fitted curves are drawn in Figs. 10 and 11. Equation (3) includes a hyperbolic tangent function and is similar to an expression used to describe the thickness of domain walls in ferroelectrics [20]. This suggests that the present suspended transition might be explained by the boundary and strain energies of a domain which has not been confirmed in malonic acid.

Another measurement was made in the $\gamma \rightarrow \beta$ transition region of MA-*d*, and the results are plotted in Fig. 12. The process of measurement is as

TABLE 7

Optimized parameters of eqn. (3)

Parameter	$CH_2(COOH)_2$	$CD_2(COOD)_2$
$P(1)$ (K)	44.3	57.8
$P(2)$	0.312	0.760

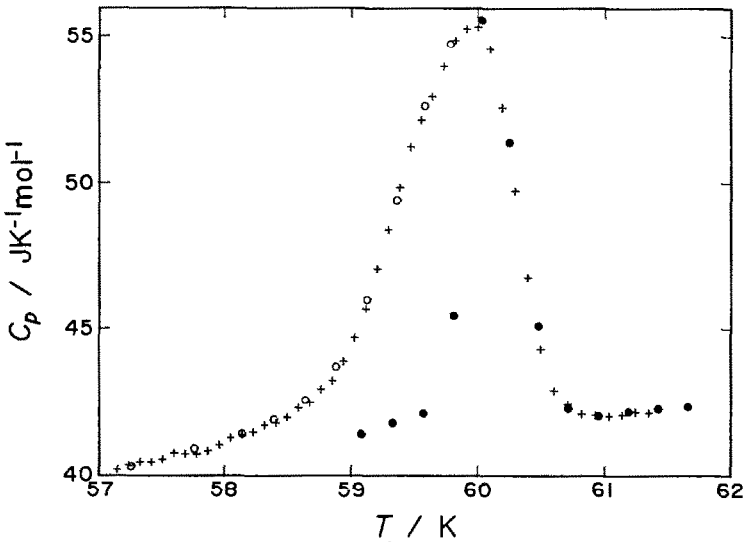

Fig. 12. Heat capacity of malonic acid-d_4 (MA-d) exhibiting the split $\gamma \rightarrow \beta$ transition peak: ○, first series (57.01–59.87 K); ●, second series (58.94–61.78 K). The process of the measurement is described in the text in detail. The data in series 6 (+) are also plotted for comparison.

follows. The sample was cooled from 62.91 to 53.91 K where the $\beta \rightarrow \gamma$ transition takes place fully according to Fig. 11. After heating the sample to 57.01 K, we started the first series of measurements (open circles in Fig. 12). After the measurement was continued up to 59.87 K, the sample was again cooled down to 58.94 K. The subsequent measurement was continued up to 61.78 K (solid circles). Figure 12 also includes the data in series 6 which were taken with the smallest temperature increment. The split transition peak thus obtained indicates that the sample memorized the temperature at which the $\gamma \rightarrow \beta$ transition was interrupted. In other words, each part of the crystal has its own $\gamma \rightarrow \beta$ transition temperature. This also explains the fact that the transition can be stopped at any intermediate stage within a temperature range in the cooling direction.

High temperature $\beta \rightarrow \alpha$ transitions

Determination of normal heat capacities and thermodynamic quantities of the $\beta \rightarrow \alpha$ transitions

The $\beta \rightarrow \alpha$ transitions are sharp first-order transitions. It is therefore not difficult to determine normal heat capacities for evaluation of the transition enthalpies and entropies. As shown previously in Figs. 4 and 5, the heat capacities of the α and β phases have their respective linear temperature dependences and there is a difference between them at the transition point. Accordingly, we fitted linear functions in T to the experimental heat

TABLE 8

Thermodynamic quantities of the $\beta \rightarrow \alpha$ transitions in $CH_2(COOH)_2$ and $CD_2(COOD)_2$

	$CH_2(COOH)_2$	$CD_2(COOD)_2$
T_{trs} (K)	352.2	348.0
$\Delta_{trs}H$ (kJ mol^{-1})	1.837 ± 0.021	1.810 ± 0.001
$\Delta_{trs}S$ (J K^{-1} mol^{-1})	5.217 ± 0.058	5.201 ± 0.001

capacities of the α and β phases separately. They are represented by the broken lines in Figs. 4 and 5.

The thermodynamic quantities of the $\beta \rightarrow \alpha$ transitions are listed in Table 8. The deuteration decreased the $\beta \rightarrow \alpha$ transition temperature slightly. In the next section, we will discuss the shift of the $\beta \rightarrow \alpha$ transition temperature due to the deuteration, together with that for the $\gamma \rightarrow \beta$ transition by using a thermodynamic model. The transition entropies of the two compounds were the same within the experimental errors and the magnitudes are comparable with R ln 2. Entropy changes of this magnitude are usually ascribed to order–disorder-type mechanisms. However, the IR and Raman spectra suggested that the α phase does not involve any disorder [9]. These large transition entropies will be discussed with a harmonic oscillator model in the next section.

Discussion of the $\beta \rightarrow \alpha$ transition enthalpies and entropies using a harmonic oscillator model

The IR and Raman spectra revealed that many vibrational frequencies of malonic acids change discontinuously at the $\beta \rightarrow \alpha$ transition points [9]. The discontinuous changes in frequencies lead to discontinuous changes in the thermodynamic properties of the crystal. We assumed that the thermodynamic quantities of the α and β phases could be expressed by the Einstein functions, i.e. the crystal lattice was regarded as a collection of harmonic oscillators, and calculated their changes due to the frequency changes at the transition temperature. The process of the calculation is described below and illustrated by the case of MA in Fig. 13.

Firstly, the entropies of the α and β phases were assumed to be zero at 0 K in accordance with the third law of thermodynamics, i.e. both phases were regarded as ordered. We computed the entropy, internal energy and free energy of each phase at the transition temperature by summing the respective Einstein functions over the vibrational frequencies listed in Table 1 of ref. 9. These quantities were calculated for 1 mol of the unit cell of the β phase which contains two molecules. There are 66 vibrational modes per unit cell. In the calculation, however, we used 38 and 39 frequencies from the spectroscopic data for MA and MA-*d* respectively, because the complete

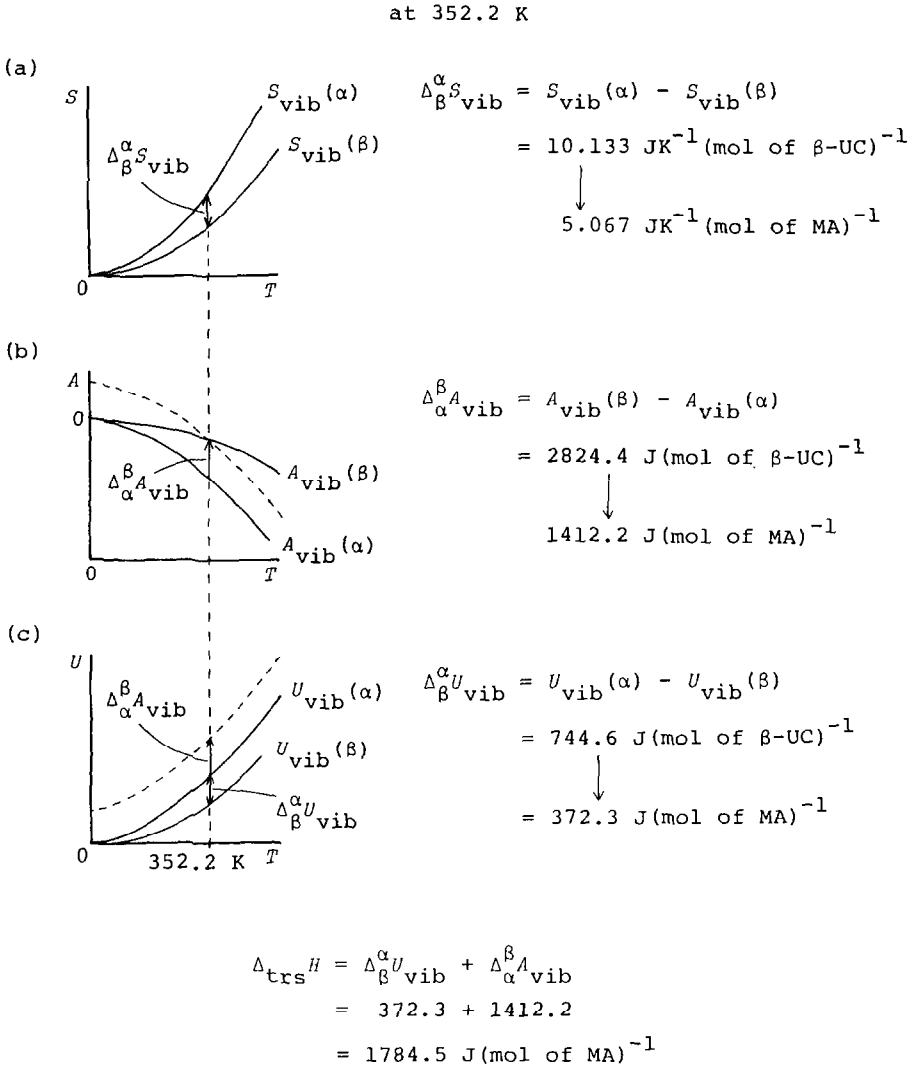

Fig. 13. Computation of the $\beta \rightarrow \alpha$ transition enthalpy and entropy of malonic acid by a harmonic oscillator model: MA, malonic acid ($CH_2(COOH)_2$); β-UC, unit cell of the β phase.

frequency data were not given in the table cited above. Most of the frequencies not used in the calculation are those due to methylenic hydrogen atoms and skeletal C–C bonds, which are insensitive to the $\beta \rightarrow \alpha$ transition. Therefore their exclusion from the calculation makes no significant contribution to the relative stability of the phases.

The difference between the entropies of the two phases was then divided by two for the reduction to units per 1 mol of malonic acid molecules. Molar internal and free energies were similarly calculated.

TABLE 9

Comparison between experimental and calculated values of the thermodynamic quantities of the $\beta \rightarrow \alpha$ transitions

		$CH_2(COOH)_2$	$CD_2(COOD)_2$
T_{trs} (K)		352.2	348.0
$\Delta_{trs}H$ (kJ mol^{-1})	Expt.	1.837	1.810
	Calc.	1.785	1.515
$\Delta_{trs}S$ (J K^{-1} mol^{-1})	Expt.	5.217	5.201
	Calc.	5.067	4.354
Calc./expt.		0.97	0.84

As the zero of the free energies is fixed at 0 K, the vibrational free energy of the α phase is lower than that of the β phase, because the vibrational frequencies are lower in the α phase than in the β phase. But the free energy curves of the two phases must cross at the first-order transition point. In other words, the free energy of the α phase must be shifted by $\Delta_{\alpha}^{\beta}A_{vib}$ as indicated by the arrow in Fig. 13(b). The vibrational free energy difference $\Delta_{\alpha}^{\beta}A_{vib}$ was thus compensated by a shift in the internal energy of the α phase (see Fig. 13(c)). There is a difference in the vibrational internal energy itself between the two phases ($\Delta_{\beta}^{\alpha}U_{vib}$). The transition enthalpy is therefore given by the sum of $\Delta_{\beta}^{\alpha}U_{vib}$ and $\Delta_{\alpha}^{\beta}A_{vib}$. Here we ignored the difference between enthalpy and internal energy.

The transition enthalpies and entropies thus calculated are compared with the experimental ones in Table 9. The calculated values cover a greater part of the experimental ones. Accordingly the experimental $\beta \rightarrow \alpha$ transition enthalpies and entropies can be attributed to the frequency changes of the normal vibrations at the transitions. This supports displacive mechanisms of the $\beta \rightarrow \alpha$ transitions which were suggested by the temperature dependence of the two Raman lattice bands [9].

Hysteresis of the $\beta \rightarrow \alpha$ transitions

We found that the β phases superheat as shown by the open circles in Figs. 14 and 15 where the enthalpies are plotted against temperature. If a first-order transition occurs ideally, enthalpy should jump at the transition temperature. In fact, the enthalpy increased smoothly up to around 2 K above the transition point. The superheated sample was then stabilized along the path represented by the broken curve in Figs. 14 or 15. During the stabilization, the sample temperature decreased despite energy input, and accordingly the apparent heat capacity was negative. We defined the "equilibrium" transition point as the temperature toward which the stabilization advanced.

The α phases supercooled as denoted by solid circles in Figs. 14 and 15. To investigate whether or not the α and β phases coexist in the same way as

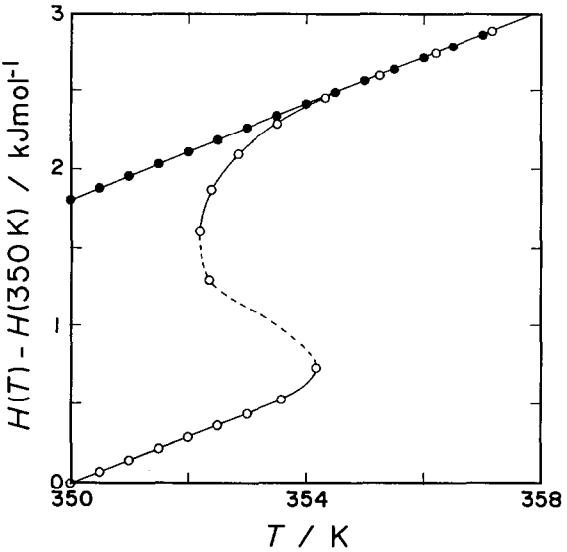

Fig. 14. Enthalpy of malonic acid (MA) near the $\beta \rightarrow \alpha$ transition: ○, series 16 (showing superheating of the β phase); ●, series 17 (supercooling of the α phase).

the β and γ phases do at the low temperature transitions, we cooled the α phase of MA to different temperatures.

When the α phase was cooled down to 338.6 K, it completely supercooled (series 17 in Figs. 4 and 14). Next, we cooled the α phase to 337.4 K. When the adiabatic condition was established after the rapid cooling, spontaneous

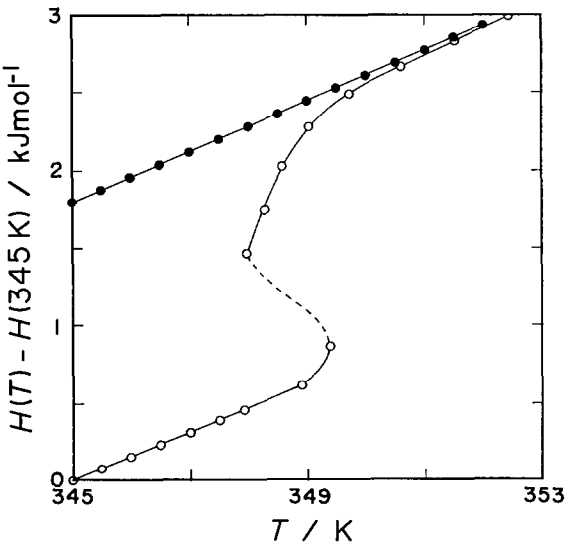

Fig. 15. Enthalpy of malonic acid-d_4 (MA-d) near the $\beta \rightarrow \alpha$ transition: ○, series 21 (showing superheating of the β phase); ●, series 22 (supercooling of the α phase).

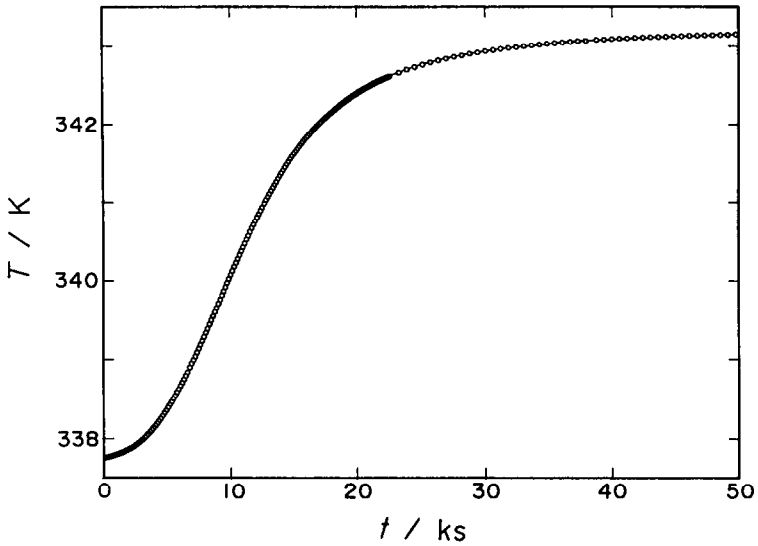

Fig. 16. A spontaneous exothermic temperature drift after rapid cooling of the α phase of malonic acid (MA) from 370.3 to 337.4 K.

heat evolution was observed to take place as the α phase transformed into the β phase. The exothermic temperature drift recorded is shown in Fig. 16. After the spontaneous heat evolution ceased, the heat capacity was measured up to 371 K. The sample underwent the $\beta \rightarrow \alpha$ transition with an enthalpy change of 1.692 kJ mol^{-1} which is 92% of the total transition enthalpy (1.837 kJ mol^{-1}). The decrease of 8% in the transition enthalpy could be ascribed to decomposition of the sample, inferred from the fact that the heat capacities of the α phase obtained in this measurement deviated by 5–8% from the data in the previous measurement. These observations indicate that there is a low temperature limit of existence of the supercooled α phase. Below the limit, the α phase cannot exist metastably in the supercooled state and transforms irreversibly into the stable β phase, leaving no trace of the α phase.

Deuteration effects on the $\gamma \rightarrow \beta$ and $\beta \rightarrow \alpha$ transition temperatures and entropies

The deuteration of MA changes the two first-order transition temperatures in opposite directions. This can be understood qualitatively by the use of free energy curves of the three phases, which are drawn schematically in Fig. 17. A first-order transition point is given by an intersection of the free energy curves of the two phases, and a transition entropy is equal to a difference in the slopes of the two curves at the transition point. Deuteration modifies the stabilities of the phases in a variety of ways that differ from phase to phase. In MA, if we assume that the deuteration makes the β phase

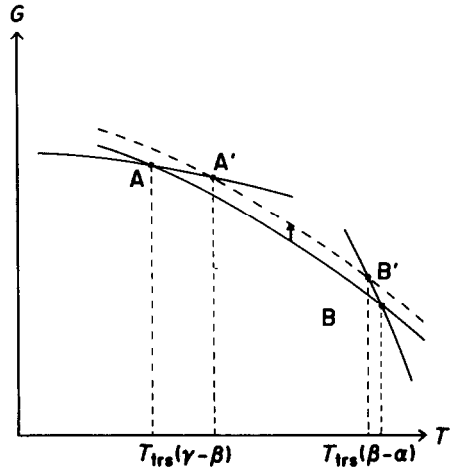

Fig. 17. Schematic diagram of the free energies of the three phases of malonic acid.

unstable, as indicated by the arrow in the figure, then the $\gamma \rightarrow \beta$ transition temperature becomes higher (A $\rightarrow$ A′) and the $\beta \rightarrow \alpha$ transition temperature lower (B $\rightarrow$ B′).

To examine the above argument quantitatively, we made the following calculation. Firstly, the free energy curves of the three phases of MA were computed from the heat capacity data. Next, the free energy curve of the β phase was shifted uniformly by the difference in the $\gamma \rightarrow \beta$ transition enthalpies of MA and MA-*d*, 9.06 (23.86 − 14.80) J mol^{-1}. The two transition points (A′ and B′ in Fig. 17) were 76.2 K and 348.5 K. The $\beta \rightarrow \alpha$ transition temperature thus calculated is nearly equal to the experimental value (348.0 K), whereas the calculation overestimates the deuteration effect

TABLE 10

Comparison of the deuteration effect on the transition temperatures and entropies in several hydrogen-bonded substances

Substance	T_{trs} (K)			$\Delta_{trs}S$ (J K^{-1} mol^{-1})			Ref.
	H	D	D/H	H	D	D/H	
H_2O	72.0	75.9	1.054	2.33	2.06	0.884	21, 22
$SnCl_2 \cdot 2H_2O$	217.94	234.47	1.076	4.6	4.6	1.0	23
$K_4[Fe(CN)_6] \cdot 3H_2O$	247.8	252.7	1.020	12.41	14.36	1.157	14
$Cu(HCO_2)_2 \cdot 4H_2O$	235.78	245.64	1.042	3.546	3.814	1.076	24
KH_2PO_4	122.7	220.0	1.793	3.51	3.520	1.003	25, 26
NH_4Br ($\delta \rightarrow \gamma$)	108.5	168.5	1.553	1.2	–	–	16
($\gamma \rightarrow \beta$)	234.8	215.5	0.918	2.6	–	–	
$(NH_4HC_2O_4)_2 \cdot H_2O$	145.4	160.1	1.101	6.01	8.23	1.369	27
$CH_2(COOH)_2$ ($\gamma \rightarrow \beta$)	47.3	60.0	1.268	0.313	0.411	1.313	This work
($\beta \rightarrow \alpha$)	352.2	348.0	0.988	5.217	5.201	0.997	

on the $\gamma \rightarrow \beta$ transition temperature. This model explains the experimental results qualitatively, but for a quantitative argument, it has to be elaborated by considering other factors such as the temperature dependence of the vibrational frequencies and the thermal volume expansion.

The deuteration effects on the transition temperatures and entropies in malonic acid are compared with those in other hydrogen-bonded substances in Table 10. These phase transitions may be divided into three groups by the magnitudes of the deuteration effects on the transition temperatures. The transitions in the first group are characterized by their relative insensitivity to deuteration. The transitions in H_2O and in some compounds having crystal water belong to this group. The second consists of those which are strongly affected by deuteration, as represented by the ferroelectric transition in KH_2PO_4. The third group is intermediate between the first and second, i.e. it comprises the transitions whose deuteration effects are moderately large. In accordance with this classification, the $\gamma \rightarrow \beta$ and $\beta \rightarrow \alpha$ transitions in malonic acid belong to the third group and first group respectively. This indicates that the $\gamma \rightarrow \beta$ transition occupies an intermediate position between classical systems such as the transition in H_2O and quantum systems such as the ferroelectric transition in KH_2PO_4 where the dynamical aspect of molecular motion is believed to play a significant role in the bulk property. In contrast, the $\beta \rightarrow \alpha$ transition seems to be of classical type.

The phase transitions in hydrogen-bonded substances can be similarly classified according to the magnitudes of the effects on the transition entropies. In malonic acid, the deuteration has no effect on the $\beta \rightarrow \alpha$ transition entropy while it affects considerably the $\gamma \rightarrow \beta$ transition entropy. It is very difficult to relate the deuteration effects on the transition entropies to the character of the transitions, because this requires a full statistical-mechanical treatment of the crystal, taking into account a large number of degrees of freedom. However, it is noteworthy that the $\gamma \rightarrow \beta$ transition entropies are the smallest among all the transitions for which relatively large deuteration effects have been previously reported.

Calculations of the standard thermodynamic functions

The standard thermodynamic functions of MA and MA-*d* are listed in Tables 11 and 12 respectively. They were calculated from polynomials fitted to the experimental heat capacities and the transition enthalpies and entropies. The values at 10 K were extrapolated by combining the Debye and Einstein functions.

TABLE 11

Standard thermodynamic functions of malonic acid

T (K)	$C_p^{\ominus}(R)$	$H^{\ominus}(T)-H^{\ominus}(0)(RT)$	$S^{\ominus}(T)-S^{\ominus}(0)(R)$	$-[G^{\ominus}(T)-H^{\ominus}(0)]\times(RT)$
10 [a]	0.1416	0.03591	0.04795	0.01204
20	0.8146	0.2369	0.3250	0.08810
30	1.855	0.5964	0.8441	0.2477
40	2.960	1.050	1.531	0.4801
Phase transition at 47.3 K				
50	3.961	1.570	2.339	0.7684
60	4.821	2.042	3.139	1.097
70	5.558	2.493	3.939	1.446
80	6.199	2.917	4.724	1.807
90	6.772	3.314	5.488	2.173
100	7.294	3.686	6.228	2.542
110	7.780	4.037	6.947	2.910
120	8.237	4.368	7.643	3.276
130	8.672	4.682	8.320	3.638
140	9.092	4.982	8.978	3.996
150	9.499	5.270	9.619	4.349
160	9.899	5.547	10.25	4.698
170	10.29	5.814	10.86	5.043
180	10.69	6.074	11.46	5.382
190	11.08	6.327	12.04	5.718
200	11.47	6.574	12.62	6.048
210	11.86	6.816	13.19	6.375
220	12.25	7.054	13.75	6.698
230	12.64	7.289	14.31	7.017
240	13.03	7.520	14.85	7.332
250	13.42	7.748	15.39	7.643
260	13.82	7.974	15.93	7.951
270	14.21	8.197	16.45	8.257
273.15	14.34	8.268	16.62	8.354
280	14.61	8.419	16.98	8.559
290	15.02	8.640	17.50	8.858
298.15	15.35	8.819	17.92	9.100
300	15.43	8.859	18.01	9.155
310	15.84	9.078	18.53	9.449
320	16.25	9.296	19.04	9.740
330	16.66	9.513	19.54	10.03
340	17.07	9.729	20.05	10.32
350	17.51	9.945	20.55	10.60
Phase transition at 352.2 K				
360	18.43	10.78	21.69	10.90
370	18.92	11.00	22.20	11.20

[a] Quantities determined by extrapolation.

TABLE 12

Standard thermodynamic functions of malonic acid-d_4

T (K)	$C_p^\ominus(R)$	$H^\ominus(T)-H^\ominus(0)(RT)$	$S^\ominus(T)-S^\ominus(0)(R)$	$-[G^\ominus(T)-H^\ominus(0)]\times(RT)$
10 [a]	0.1355	0.03404	0.04541	0.01137
20	0.8506	0.2400	0.3263	0.08633
30	1.921	0.6174	0.8681	0.2507
40	3.055	1.086	1.577	0.4911
50	4.118	1.587	2.374	0.7870
Phase transition at 60.0 K				
70	5.699	2.584	4.067	1.484
80	6.360	3.015	4.872	1.857
90	6.955	3.421	5.656	2.236
100	7.504	3.802	6.418	2.616
110	8.023	4.162	7.158	2.996
120	8.524	4.505	7.877	3.372
130	9.013	4.833	8.579	3.746
140	9.494	5.149	9.264	4.116
150	9.969	5.454	9.936	4.482
160	10.44	5.751	10.59	4.843
170	10.91	6.041	11.24	5.200
180	11.38	6.325	11.88	5.554
190	11.86	6.603	12.51	5.903
200	12.33	6.878	13.13	6.249
210	12.80	7.149	13.74	6.591
220	13.27	7.416	14.35	6.930
230	13.73	7.681	14.95	7.265
240	14.19	7.943	15.54	7.598
250	14.65	8.202	16.13	7.927
260	15.11	8.459	16.71	8.254
270	15.56	8.713	17.29	8.578
273.15	15.70	8.793	17.47	8.677
280	16.01	8.966	17.87	8.899
290	16.46	9.217	18.44	9.218
298.15	16.83	9.419	18.90	9.478
300	16.91	9.466	19.00	9.535
310	17.36	9.713	19.56	9.849
320	17.81	9.959	20.12	10.16
330	18.24	10.20	20.68	10.47
340	18.67	10.45	21.23	10.78
Phase transition at 348.0 K				
350	19.56	11.31	22.40	11.09
360	20.06	11.55	22.96	11.41
370	20.55	11.78	23.52	11.73

[a] Quantities determined by extrapolation.

CONCLUSION

The two first-order phase transitions in malonic acid have contrasting thermodynamic properties.

The $\gamma \rightarrow \beta$ transition entropies are very small and the $\beta \rightarrow \alpha$ transition entropies are comparable with R ln 2. In spite of the large difference in the magnitudes, both transition entropies are explained by displacive transition mechanisms.

The two transitions exhibit different hystereses. Both the α and β phases supercool. The supercooled α phase exists above a threshold temperature, and below that limit it transforms completely into the β phase. The $\gamma \rightarrow \beta$ transition is martensitic in nature. The supercooled β phase coexists with the γ phase in a certain temperature range, where the transition can be stopped at an intermediate stage. However, the β phase superheats whereas the γ phase does not. In addition, the $\gamma \rightarrow \beta$ transition temperature appears to have a distribution in the crystal and each part of the crystal undergoes the transition at its own transition temperature.

Deuteration has different effects on the two transitions. It increases substantially the $\gamma \rightarrow \beta$ transition temperature, while it decreases slightly the $\beta \rightarrow \alpha$ transition temperature. Moreover, it causes a remarkably large change in the $\gamma \rightarrow \beta$ transition entropy, but it does not affect the $\beta \rightarrow \alpha$ transition entropy.

At present, the molecular basis for this different behaviour is not understood.

REFERENCES

1 S. Ganguly, J.R. Fernandes, G.R. Desiraju and C.N.R. Rao, Chem. Phys. Lett., 69 (1980) 227.
2 H. Suga, unpublished work, 1978.
3 J.A. Goedkoop and C.H. MacGillavry, Acta Crystallogr., 10 (1957) 125.
4 C. Pigenet, G. Lucazeau and A. Novak, J. Chim. Phys., 73 (1976) 141.
5 R.G. Delaplane and R. Tellgren, personal communication, 1989.
6 W. Derbyshire, T.C. Gorvin and D. Warner, Mol. Phys., 17 (1969) 401.
7 C. Pigenet, G. Lucazeau and A. Novak, in Molecular Spectroscopy of Dense Phases, M. Grossmann (Ed.), Elsevier, Amsterdam, 1976, p. 311.
8 R.K. McMullan, H.P. Weber, G. Qi and B.M. Craven, Abstr. Int. Conf. on Neutron Scattering, Printing Office of Institut Laue Langevin, Grenoble, France, 1988.
9 J. de Villepin, M.H. Limage, A. Novak, N. Toupry, M. Le Postollec, H. Poulet, S. Ganguly and C.N.R. Rao, J. Raman Spectrosc., 15 (1984) 41.
10 R.G. Delaplane, The ISIS Annual Report, Rutherford Appleton Laboratory, U.K., 1989, p. A5.
11 M. Tatsumi, T. Matsuo, H. Suga and S. Seki, Bull. Chem. Soc. Jpn., 48 (1975) 3060.
12 T. Matsuo and H. Suga, Thermochim. Acta, 88 (1985) 149.
13 S. Lau, J.P. Wesson and B. Wunderlich, Macromolecules, 17 (1984) 1102.
14 M. Oguni, T. Matsuo, H. Suga and S. Seki, Bull. Chem. Soc. Jpn., 48 (1975) 379.
15 K. Moriya, T. Matsuo, H. Suga and S. Seki, Bull. Chem. Soc. Jpn., 52 (1979) 3152.

16 K. Watanabe, M. Oguni, T. Matsuo, H. Suga and S. Seki, Bull. Chem. Soc. Jpn., 55 (1982) 1003.
17 M. Oguni, K. Watanabe, T. Matsuo and H. Suga, Thermochim. Acta, 74 (1984) 331.
18 M. Yoshikawa, M. Sorai, H. Suga and S. Seki, J. Phys. Chem. Solids, 44 (1983) 311.
19 N. Onoda, T. Matsuo and H. Suga, Philos. Mag. A, 57 (1988) 245.
20 V.A. Zhirnov, Sov. Phys. JETP, 35 (1959) 822.
21 Y. Tajima, T. Matsuo and H. Suga, J. Phys. Chem. Solids, 45 (1984) 1135.
22 T. Matsuo, Y. Tajima and H. Suga, J. Phys. Chem. Solids, 47 (1986) 165.
23 T. Matsuo, M. Oguni, H. Suga, S. Seki and J.F. Nagle, Bull. Chem. Soc. Jpn., 47 (1974) 57.
24 T. Matsuo, Y. Kume, H. Suga and S. Seki, J. Phys. Chem. Solids, 37 (1976) 499.
25 W. Reese and L.F. May, Phys. Rev., 162 (1967) 510.
26 W. Reese and L.F. May, Phys. Rev., 167 (1968) 504.
27 M. Fukai, T. Matsuo and H. Suga, J. Phys. Chem. Solids, 50 (1989) 743.